

MIT Open Access Articles

Photo-induced trimming of chalcogenide-assisted silicon waveguides

The MIT Faculty has made this article openly available. **Please share** how this access benefits you. Your story matters.

Citation: Canciamilla, Antonio et al. "Photo-induced Trimming of Chalcogenide-assisted Silicon Waveguides." *Optics Express* 20.14 (2012): 15807. © 2012 OSA

As Published: <http://dx.doi.org/10.1364/OE.20.015807>

Publisher: Optical Society of America

Persistent URL: <http://hdl.handle.net/1721.1/79747>

Version: Final published version: final published article, as it appeared in a journal, conference proceedings, or other formally published context

Terms of Use: Article is made available in accordance with the publisher's policy and may be subject to US copyright law. Please refer to the publisher's site for terms of use.



Photo-induced trimming of chalcogenide-assisted silicon waveguides

Antonio Canciamilla,^{1,*} Francesco Morichetti,¹ Stefano Grillanda,¹
Philippe Velha,² Marc Sorel,² Vivek Singh,³ Anu Agarwal,³
Lionel C. Kimerling,³ and Andrea Melloni¹

¹Dipartimento di Elettronica e Informazione, Politecnico di Milano, Milano, Italy

²School of Engineering, University of Glasgow, Glasgow G12 8LT, UK

³Microphotonics Center, Massachusetts Institute of Technology, Cambridge, MA 02139, USA

*canciamilla@elet.polimi.it

Abstract: A chalcogenide-assisted silicon waveguide is realized by depositing a thin layer of A_2S_3 glass onto a conventional silicon on insulator optical waveguide. The photosensitivity of the chalcogenide is exploited to locally change the optical properties of the waveguide through exposure to visible light radiation. Waveguide trimming is experimentally demonstrated by permanently shifting the resonant wavelength of a microring resonator by 6.7 nm, corresponding to an effective index increase of $1.6 \cdot 10^{-2}$. Saturation effects, trimming range, velocity and temporal stability of the process are discussed in details. Results demonstrate that photo-induced treatments can be exploited for a post-fabrication compensation of fabrication tolerances, as well as to set and reconfigure the circuit response.

© 2012 Optical Society of America

OCIS codes: (130.3120) Integrated optics devices; (130.3130) Integrated optics materials; (160.5335) Photosensitive materials; (230.1150) All-optical devices; (250.5300) Photonic integrated circuits.

References and links

1. R. A. Soref and B. R. Bennett, "Electrooptical effects in silicon," *IEEE J. Quantum Electron.* **23**, 123-129 (1987).
2. D. A. B. Miller, "Optical interconnects to silicon," *IEEE J. Sel. Top. Quantum Electron.* **6**, 1312-1317 (2000).
3. B. Jalali, M. Paniccia, and G. Reed, "Silicon photonics," *IEEE Microw. Mag.* **7**, 58-68 (2006).
4. C. Ferrari, A. Canciamilla, F. Morichetti, M. Sorel, and A. Melloni, "Penalty-free transmission in a silicon coupled resonator optical waveguide over the full C-band," *Opt. Lett.* **36**, 3948-3950 (2011).
5. S. Ibrahim, N. K. Fontaine, S. S. Djordjevic, B. Guan, T. Su, S. Cheung, R. P. Scott, A. T. Pomerene, L. L. Seaford, C. M. Hill, S. Danziger, Z. Ding, K. Okamoto, and S. J. B. Yoo, "Demonstration of a fast-reconfigurable silicon CMOS optical lattice filter," *Opt. Express* **19**, 13245-13256 (2011).
6. A. Melloni, A. Canciamilla, C. Ferrari, F. Morichetti, L. O'Faolain, T. F. Krauss, R. De La Rue, A. Samarelli, and M. Sorel, "Tunable delay lines in silicon photonics: coupled resonators and photonic crystals, a comparison," *IEEE Photon. J.* **2**, 181-194 (2010).
7. Q. Xu, S. Manipatruni, B. Schmidt, J. Shakya, and M. Lipson, "12.5 Gbit/s carrier-injection-based silicon microring silicon modulators," *Opt. Express* **15**, 430-436 (2007).
8. H. Rong, R. Jones, A. Liu, O. Cohen, D. Hak, A. Fang, and M. Paniccia, "A continuous-wave Raman silicon laser," *Nature (London)* **433**, 292-294 (2005).
9. D. Ahn, C. Y. Hong, J. Liu, W. Giziewicz, M. Beals, L. C. Kimerling, J. Michel, J. Chen, and F. X. Kärtner, "High performance, waveguide integrated Ge photodetectors," *Opt. Express* **15**, 3916-3921 (2007).
10. F. Morichetti, A. Canciamilla, C. Ferrari, A. Samarelli, M. Sorel, and A. Melloni, "Travelling-wave resonant four-wave mixing breaks the limits of cavity-enhanced all-optical wavelength conversion," *Nat. Commun.* **2**, 296 (2011).
11. A. Canciamilla, M. Torregiani, C. Ferrari, F. Morichetti, R. M. De La Rue, A. Samarelli, M. Sorel, and A. Melloni, "Silicon coupled-ring resonator structures for slow light applications: potential, impairments and ultimate limits," *J. Opt.* **12**, 104008 (2010).

12. M. A. Popovic, T. Barwicz, E. P. Ippen, and F. X. Kärtner, "Global design rules for silicon microphotonic waveguides: sensitivity, polarization and resonance tunability," in *Conference on Lasers and Electro-Optics/Quantum Electronics and Laser Science Conference and Photonic Applications Systems Technologies*, Technical Digest (CD) (Optical Society of America, 2006), paper CTuCC1.
13. F. Morichetti, A. Canciamilla, C. Ferrari, M. Torregiani, A. Melloni, and M. Martinelli, "Roughness induced backscattering in optical silicon waveguides," *Phys. Rev. Lett.* **104**, 033902 (2010).
14. F. Morichetti, A. Canciamilla, M. Martinelli, A. Samarelli, R. M. De La Rue, M. Sorel, and A. Melloni, "Coherent backscattering in optical microring resonators," *Appl. Phys. Lett.* **96**, 081112 (2010).
15. C. Ferrari, F. Morichetti, and A. Melloni, "Disorder in coupled-resonator optical waveguides," *J. Opt. Soc. Am. B* **26**, 858–866 (2009).
16. J. Schrauwen, D. van Thourhout, and R. Baets, "Trimming of silicon ring resonator by electron beam induced compaction and strain," *Opt. Express* **16**, 3738–3743 (2008).
17. Y. Shen, I. B. Divliansky, D. N. Basov, and S. Mookherjee, "Electric-field-driven nano-oxidation trimming of silicon microrings and interferometers," *Opt. Lett.* **36**, 2668–2670 (2011).
18. C. J. Chen, J. Zheng, T. Gu, J. F. McMillan, M. Yu, G. Q. Lo, D. L. Kwong, and C. W. Wong, "Selective tuning of high-Q silicon photonic crystal nanocavities via laser-assisted local oxidation," *Opt. Express* **19**, 12480–12489 (2011).
19. D. Bachman, Z. Chen, A. M. Prabhu, R. Fedosejevs, Y. Y. Tsui, and V. Van, "Femtosecond laser tuning of silicon microring resonators," *Opt. Lett.* **36**, 4695–4697 (2011).
20. S. T. Chu, W. Pan, S. Sato, T. Kaneko, B. Little, and Y. Kokubun, "Wavelength trimming of a microring resonator filter by means of a UV sensitive polymer overlay," *IEEE Photon. Technol. Lett.* **11**, 688–690 (1999).
21. D. K. Sparacin, C. Hong, L. C. Kimerling, J. Michel, J. P. Lock, and K. K. Gleason, "Trimming of microring resonators by photo-oxidation of a plasma-polymerized organosilane cladding material," *Opt. Lett.* **30**, 2251–2253 (2005).
22. B. J. Eggleton, B. Luther-Davies, and K. Richardson, "Chalcogenide photonics," *Nat. Photonics* **5**, 141–148 (2011).
23. S. J. Madden, D. Y. Choi, M. R. E. Lamont, V. G. Ta'eed, N. J. Baker, M. D. Pelusi, B. Luther-Davies, and B. J. Eggleton, "Chalcogenide glass photonic chips," *Opt. Photonics News* **19**, 18–23 (2008).
24. A. van Popta, R. DeCorby, C. Haugen, T. Robinson, J. McMullin, D. Tonchev, and S. Kasap, "Photoinduced refractive index change in As₂Se₃ by 633nm illumination," *Opt. Express* **10**, 639–644 (2002).
25. A. Zakery and S. R. Elliott, "Optical properties and applications of chalcogenide glasses: a review," *J. Non-Cryst. Solids* **330**, 1–12 (2003).
26. N. Hô, M. Phillips, H. Qiao, P. Allen, K. Krishnaswami, B. Riley, T. Myers, and N. Anheier, "Single-mode low-loss chalcogenide glass waveguides for the mid-infrared," *Opt. Lett.* **31**, 1860–1862 (2006).
27. A. Salimonia, A. Villeneuve, T. V. Galstyan, S. La Rochelle, and K. Richardson, "First- and second-order Bragg gratings in single-mode planar waveguides of chalcogenide glasses," *J. Lightwave Technol.* **17**, 837–842 (1999).
28. M. W. Lee, C. Grillet, C. L. Smith, D. J. Moss, B. J. Eggleton, D. Freeman, B. Luther-Davies, S. Madden, A. Rode, Y. Ruan, and Y. H. Lee, "Photosensitive post tuning of chalcogenide photonic crystal waveguides," *Opt. Express* **15**, 1277–1285 (2007).
29. N. Carlie, J. D. Musgraves, B. Zdyrko, I. Luzinov, J. Hu, V. Singh, A. Agarwal, L. C. Kimerling, A. Canciamilla, F. Morichetti, A. Melloni, and K. Richardson, "Integrated chalcogenide waveguide resonators for mid-IR sensing: leveraging material properties to meet fabrication challenges," *Opt. Express* **18**, 26728–26743 (2010).
30. A. Canciamilla, S. Grillanda, F. Morichetti, C. Ferrari, J. Hu, J. D. Musgraves, K. Richardson, A. Agarwal, L. C. Kimerling, and A. Melloni, "Photo-induced trimming of coupled ring-resonator filters and delay lines in As₂S₃ chalcogenide glass," *Opt. Lett.* **36**, 4002–4004 (2011).
31. M. Gnan, S. Thorns, D. S. Macintyre, R. M. De La Rue, and M. Sorel, "Fabrication of low-loss photonic wires in silicon-on-insulator using hydrogen silsesquioxane electron-beam resist," *Electron. Lett.* **44**, 115–116 (2008).
32. F. Xia, L. Sekaric, and Y. Vlasov, "Ultracompact optical buffers on a silicon chip," *Nat. Photonics* **1**, 65–71 (2007).
33. J. Hu, N. Carlie, N. N. Feng, L. Petit, A. Agarwal, K. Richardson, and L. Kimerling, "Planar waveguide-coupled, high-index-contrast, high-Q resonators in chalcogenide glass for sensing," *Opt. Lett.* **33**, 2500–2502 (2008).
34. T. V. Galstyan, J. -F. Viens, A. Villeneuve, K. Richardson, and M. A. Duguay, "Photoinduced self-developing relief gratings in thin film chalcogenide As₂S₃ glasses," *J. Lightwave Technol.* **15**, 1343–1347 (1997).
35. D. Ielmini, A. L. Lacaita, and D. Mantegazza, "Recovery and drift dynamics of resistance and threshold voltages in phase-change memories," *IEEE Trans. Electron Devices* **54**, 308–315 (2007).
36. J. Hu, M. Torregiani, F. Morichetti, N. Carlie, A. Agarwal, K. Richardson, L. C. Kimerling, and A. Melloni, "Resonant cavity-enhanced photosensitivity in As₂S₃ chalcogenide glass at 1550 nm telecommunication wavelength," *Opt. Lett.* **35**, 874–876 (2010).
37. M. A. Popovic, T. Barwicz, M. S. Dahlem, F. Gan, C. W. Holzwarth, P. T. Rakich, H. I. Smith, E. P. Ippen, and F. X. Kärtner, "Tunable, fourth-order silicon microring-resonator add-drop filters," in *33rd European Conference and Exhibition of Optical Communication (ECOC)*, IET Seminar Digests (2007), paper 123.

1. Introduction

Silicon-on-insulator (SOI) is emerging as the leading material system to realize on-chip densely integrated photonic circuits with advanced functionalities [1–3]. A wide set of both passive and active devices, working in linear and nonlinear regimes, have recently been demonstrated [4–10], showing the potential of this technology for optical processing, sensing and interconnects.

Besides the intrinsic compatibility with devices and manufacturing processes of microelectronics, the main advantage of silicon photonics is the strong light confinement offered by the high refractive index contrast, that enables photonic integrated circuits (PICs) with large bandwidth, high selectivity and ultra-small footprint.

However, the high index contrast and the sub-micrometer waveguide dimensions are also responsible for a strong sensitivity to fabrication tolerances, currently representing the main constraint of SOI PICs. Considering for example a typical single-mode waveguide, a width deviation of only 1 nm causes an effective index variation of $2 \cdot 10^{-3}$, producing a frequency shift of about 100 GHz in the spectral response of any interferometric device [11, 12]. Even for most advanced and highly accurate fabrication processes, these figures pose huge technological challenges and severe design constraints, especially for resonant, multi-stages or high-quality-factor devices [11, 13–15].

Post-fabrication treatments, able to finely tailor the local properties of SOI PICs, are therefore mandatory to compensate for unavoidable fabrication inaccuracies in order to recover the desired specifications and functionalities. Moreover, they also open the way to the realization of PICs with reconfigurable transfer function. Active tuning techniques, such as local heating through thermo-optic actuators [6] or carrier injection through p-i-n junctions [5], are commonly used. Nevertheless they require complex additional fabrication steps and, being based on “always-on” mechanisms, are inherently power-hungry and poorly efficient when continuous and fast reconfiguration is not required.

Permanent trimming techniques, where the induced refractive index change does not disappear when the applied trimming source is switched off, have recently attracted great interest. The trimming of SOI microring resonators has been demonstrated by exploiting the oxide compaction induced by electron beam exposure [16] or the silicon oxidation induced by the tip of an atomic force microscope [17]. Although large (up to $1.3 \cdot 10^{-2}$) effective index variations can be achieved, these techniques require sophisticated, expensive and power-consuming equipment, that is hardly in line with low-cost manufacturing and makes real-time monitoring of the process difficult. A more flexible solution, successfully applied to both SOI photonic crystal cavities [18] and microring resonators [19], is the use of a highly localized laser beam to selectively induce oxidation, amorphization or nanomilling of the silicon surface. Nevertheless it needs very high energy density (in the order of 10^8 and 10^{15} mW/cm², respectively) and is affected by transient thermo-optic and surface chemistry effects. Alternative techniques, used on different high index contrast technological platforms, employ UV sensitive polymer films as waveguide cladding [20, 21], whose refractive index is tailored by local UV exposure. Besides requiring a UV-source for the trimming, most polymers suffer from poor temporal stability and optical degradation at relatively low temperatures.

In this work we propose an innovative approach to realize trimmable silicon PICs. Chalcogenide-assisted silicon waveguides are made by depositing As_2S_3 glass as upper cladding in an otherwise standard SOI process. The photosensitivity of chalcogenide glass (ChGs) materials is then exploited to selectively tailor the local optical properties of the waveguides, by using nothing more than a low-intensity visible-light source. The trimming technique is simple, accurate, low-cost, and permanent, enabling compensation for fabrication tolerances and reconfiguration of the circuit transfer function. We investigate in detail its performance by trimming the resonance frequency of a silicon micro-ring resonator: saturation effects, ve-

locity and temporal stability of the process are characterized and the optimum design of the ChG-assisted SOI waveguide is discussed.

2. Chalcogenide-assisted silicon waveguide

ChGs are a class of amorphous semiconductor compounds that are emerging as promising materials for PICs [22, 23]. Their photosensitivity in the visible region of the spectrum is well known [24]: band gap illumination is able to modify the chemical bonds and the local atomic structure of the material, originating the photo-darkening effect [22, 25]. Besides a red-shift of the absorption edge toward the visible wavelength region, this phenomenon produces also an increasing of the refractive index in the transparent wavelength region (near IR). This property has been used not only to directly write optical waveguides [26] and Bragg gratings [27] on a ChG platform, but, more recently, also to adjust the optical properties of ChG devices, such as photonic crystal cavities [28] and complex ring resonator based structures [29, 30]. In particular, we experimentally demonstrated that the effective index of an As_2S_3 waveguide can be changed up to $\Delta n_{eff} = 3.2 \cdot 10^{-2}$, without any saturation effect [30]. This means that the refractive index of the ChG core can be varied through exposure to visible light by at least $\Delta n_{As_2S_3} = 4 \cdot 10^{-2}$. This value is assumed in the following numerical investigations.

As_2S_3 glass is used here to realize ChG-assisted silicon waveguides with a cross section that is depicted schematically in Fig. 1(a). A typical SOI single-mode channel waveguide, optimized for TE polarization propagation, with height $h = 220$ nm and width $w = 500$ nm [31, 32], is covered by an upper cladding layer of As_2S_3 , with refractive index $n_{As_2S_3} = 2.4$ at a wavelength of 1550 nm. A photo-induced refractive index change of the As_2S_3 cladding results in a permanent variation of the effective index Δn_{eff} of the waveguide modes, making the optical properties of silicon structures easily trimmable. Moreover this Δn_{eff} produces, in any interferometric

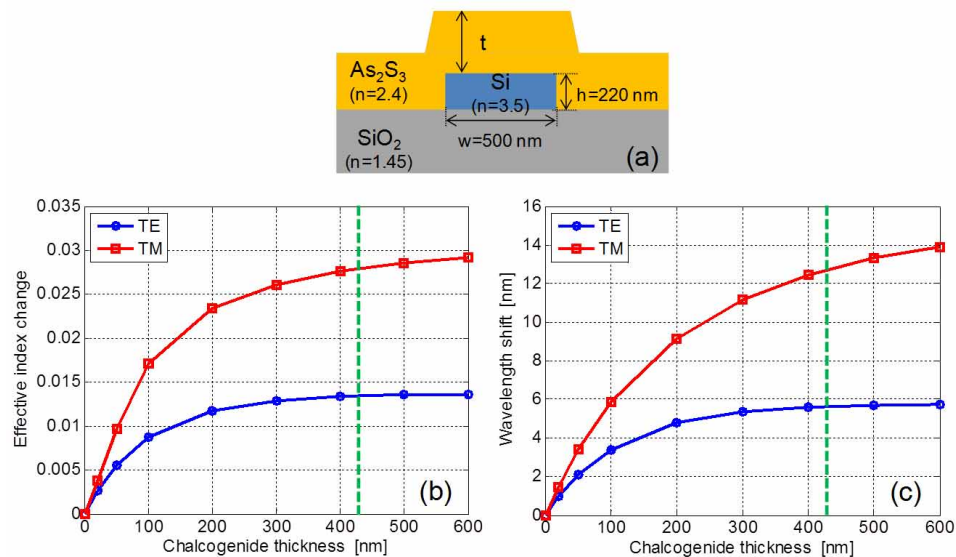


Fig. 1. ChG-assisted silicon waveguides: (a) schematic view of the waveguide cross section; (b)-(c) numerical simulations of the effects of ChG photosensitivity (for $\Delta n_{As_2S_3} = 4 \cdot 10^{-2}$): effective index variation (b) and corresponding wavelength shift (c) versus ChG thickness t , for TE (blue circles) and TM (red squares) polarizations. Green dashed line corresponds to the value selected for device fabrication ($t = 420$ nm).

device, a wavelength shift of the transfer function equal to $\Delta\lambda = \lambda_0 \Delta n_{eff} / n_g$, where λ_0 is the central wavelength and n_g is the group refractive index.

The effects of ChG photosensitivity on the waveguide propagation have been investigated through numerical electromagnetic simulations, assuming a $\Delta n_{As_2S_3}$ equal to $4 \cdot 10^{-2}$ (as above derived from [30]). Figures 1(b) and 1(c) show, respectively, the behaviour of Δn_{eff} and $\Delta\lambda$ as a function of the ChG cladding thickness t , for both TE (blue circles) and TM (red squares) polarizations.

Even a thin layer of ChG is able to provide a large trimmability of the circuits: for TE mode, for example, $t = 20$ nm enables a $\Delta\lambda$ as large as 1 nm, i.e. 125 GHz. For $t > 400$ nm, the effects of photosensitivity become poorly dependent on t . Figure 1 also shows that, given the same index change of ChG cladding, the TM-polarized fundamental mode of the waveguide is twice as sensitive as the TE-polarized fundamental mode, because of its weaker confinement factor. Therefore, depending on the specific application, the optimum polarization can be used to maximize either the trimmability of the circuits or the bandwidth and compactness of the devices.

In agreement with these considerations, ChG-assisted silicon waveguides were fabricated with an optimum As_2S_3 thickness value of $t = 420$ nm (green dashed line in Fig. 1(b) and (c)), from which we expect a waveguide sensitivity of $\partial n_{eff} / \partial n_{As_2S_3} = 0.33$, resulting in $\Delta n_{eff} = 1.3 \cdot 10^{-2}$ and $\Delta\lambda = 5.6$ nm (i.e. 700 GHz). The silicon core waveguide was patterned through electron-beam lithography and inductively coupled plasma reactive ion etching, according to the process described in [31]. In order to improve the fiber-to-waveguide coupling efficiency, the waveguide is widened up to $5 \mu\text{m}$ approaching the chip end-facets. The As_2S_3 glass cladding layer was thermally evaporated on top of the waveguide according to the process described in [33]. Figure 2(a) reports an SEM (Scanning Electron Microscope) photomicrograph of the realized waveguide cross-section at the chip end-facet, showing good uniformity and conformity of the deposition process. The 70-nm-thick layer between the silicon core and the ChG upper cladding is the HSQ (hydrogen silsesquioxane) resist used for e-beam lithography, that is not removed, since it does not significantly affect the waveguide properties.

3. Trimming of a silicon microring resonator

The trimmability of ChG-assisted silicon waveguides and circuits and the performance of the trimming technique were experimentally investigated by observing the photo-induced resonance frequency shift of a resonator. The waveguide and the fabrication process described above were used to realize the micro-ring depicted in the top view photomicrograph of Fig. 2(b). The filter has a coupling gap between the ring and the bus waveguide of 300 nm, a bending radius of $40 \mu\text{m}$ and a free spectral range (FSR) of 2.48 nm (310 GHz). Both the ring and the coupled bus waveguide are covered with 420 nm of As_2S_3 and, after fabrication, the device was stored in the dark in order to avoid any spurious light exposure. The experimental spectral

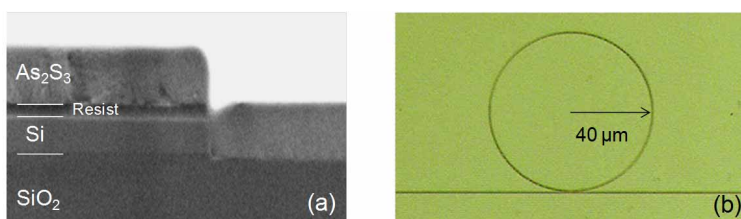


Fig. 2. Photomicrographs of the fabricated ChG-assisted silicon devices: (a) SEM image of the waveguide cross section; (b) optical microscope top view of a micro-ring resonator.

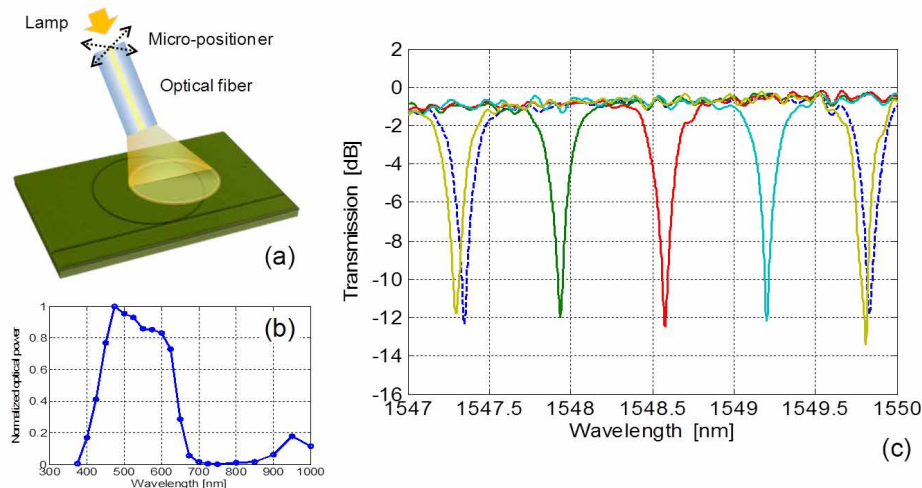


Fig. 3. (a) Schematic view of the trimming process of a ChG-assisted SOI micro-ring. (b) Normalized optical spectral density of the visible light source used for the trimming. (c) Experimental spectral response of the micro-ring: progressive photoinduced red-shift from the as-fabricated condition (blue dashed line) to 1 FSR shift (brown line).

response of the as-fabricated ring resonator (for a TE-polarized input light) is reported as the dashed blue line in Fig. 3(c), showing good filtering performance, with a -3 dB stop band of 19 GHz (0.15 nm) and an extinction ratio of 11 dB.

In order to modify the transfer function of the resonator, we locally and selectively trim the n_{eff} of the waveguide forming the ring, by using nothing more than a visible-light source and an optical fiber. According to the schematic view in Fig. 3(a), a multimode fiber with 30 μm mode field diameter was coupled to a halogen lamp and vertically positioned on top of the chip, the position of its end-facet being controlled by a micro-positioning stage in order to expose only the desired portion of the PIC. The spectral emission of the lamp, reported in Fig. 3(b), ranges from 450 nm to 650 nm wavelength and the light intensity at the fiber output can be varied from 0.3 mW/cm^2 to 10 mW/cm^2 .

The experimental results reported in Fig. 3(c) show that the light exposure is responsible for a progressive red shift of the frequency response of the ring over a whole FSR (solid lines, from green to brown). In this case, the whole waveguide forming the ring is uniformly exposed, except the coupling region to avoid coupling coefficient variations. The wavelength shift is rigid, with neither appreciable changes in the depth nor in the width of the resonant notch, thus demonstrating the lack of additional losses induced by the trimming process and the ability to avoid the exposure of the coupler.

These achievements therefore demonstrate the twofold appealing property of ChG-assisted SOI waveguides: besides enabling easy counteraction of the technological tolerances of SOI platform and restoration of the desired response of the devices, they also open the way to the realization of PICs that can be reconfigured after fabrication.

4. Performance of the trimming technique

Once we demonstrated the capability to finely trim the optical properties of ChG-assisted SOI devices, we investigated the performance of the trimming technique in terms of maximum achievable index change, saturation effects, photo-writing speed and temporal stability.

The measured wavelength shift $\Delta\lambda$ of the ring's resonance is reported in Fig. 4(a) versus the

exposure time, when the intensity of the visible light at the fiber output is $I_T = 1 \text{ mW/cm}^2$. The experimental (blue circles) and interpolated curves (red dashed line) show that the material photosensitivity moves toward saturation, enabling a maximum achievable $\Delta\lambda$ as large as 6.7 nm (i.e. about 2.5 times the FSR of the ring resonator). This corresponds to an average effective index change of $\Delta n_{eff} = 1.6 \cdot 10^{-2}$, due to an estimated refractive index variation of the ChG cladding of $\Delta n_{As_2S_3} = 4.8 \cdot 10^{-2}$. These values are in good agreement with the simulations reported in Fig. 1, based on experimental results on ChG-based PICs [30].

At $I_T = 1 \text{ mW/cm}^2$ the time constant of the whole trimming process, measured from 10% to 90% of the maximum $\Delta\lambda$, is about 400 minutes, while the trimming velocity in the linear region of the curve is about 65 pm/min, i.e. 8 GHz/min. Figures 4(b) and 4(c) compare the results of Fig. 4(a) (red dashed line) with the $\Delta\lambda$ measured over a nominally identical ring resonator (solid lines with markers), exposed to three different values of light intensity I_T : 1 mW/cm² (black circles), 2 mW/cm² (blue squares) and 3 mW/cm² (green triangles).

These experimental results show that the velocity of the trimming process scales linearly with the intensity of the incident visible light [Fig. 4(b)], since the photo-induced wavelength shift is proportional only to the exposure energy density [Fig. 4(c)]. In particular, in the unsaturated region, the resonant wavelength moves with a velocity of about $65 \cdot I_T$ pm/min (I_T being the

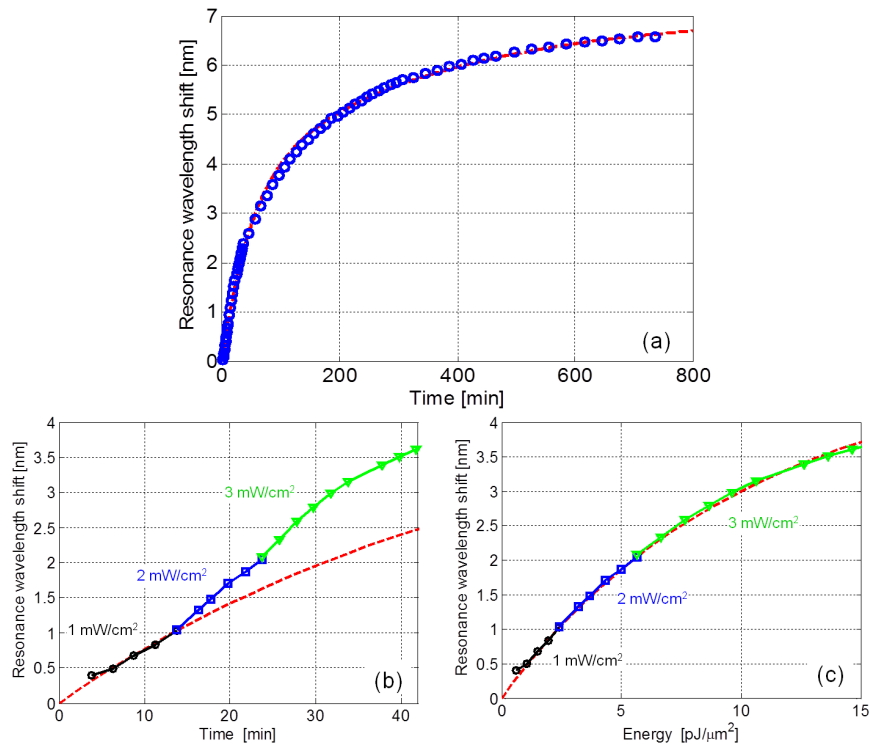


Fig. 4. Experimental behaviour of the photo-induced resonance wavelength shift of ChG-assisted SOI micro-rings: (a) versus the exposure time, when $I_T = 1 \text{ mW/cm}^2$ (blue circles); (b) versus the exposure time and (c) the exposure energy density, for different values of I_T : 1 mW/cm² (black circles), 2 mW/cm² (blue squares) and 3 mW/cm² (green triangles). Red dashed line is the interpolating curve of the experimental data in (a), reported for comparison also in (b) and (c).

light intensity in mW/cm^2 units), producing a wavelength shift $\Delta\lambda \approx 330 \cdot E_T$ pm (E_T being the light energy density in $\text{pJ}/\mu\text{m}^2$ units). This means that a wavelength shift of the ring's resonance over an entire FSR, i.e., a complete trimming or reconfiguration of the device transfer function, is achieved in about 40 minutes at $I_T = 1 \text{ mW}/\text{cm}^2$, but requires only 1 minute if a moderately low intensity of $I_T = 40 \text{ mW}/\text{cm}^2$ is used, reaching a tuning speed of 5.2 GHz/s. In both cases it requires an energy density of only $7.4 \text{ pJ}/\mu\text{m}^2$.

To check the temporal stability of the trimming process, the device described above was stored in the dark for 91 days after light exposure and periodically measured keeping the sample at the constant temperature of 25°C by means of a thermoelectric cooler. Experimental results (blue circles) in Fig. 5 reveal a small red-shift of 0.16 nm of the ring's resonance frequency, corresponding to only 2% of the wavelength shift induced by visible-light trimming. This wavelength drift is due to the structural relaxation experienced by ChG materials after exposure to light at photon energy above the band gap [27,34]. Its temporal evolution is consistent with a power-law description (red curve in Fig. 5), that is commonly used in literature to model the drift of the electrical parameters of ChG materials [35].

Regarding the magnitude of the wavelength drift, preliminary experiments suggest that it depends on the overall induced wavelength shift. This means that a wavelength shift lower than a FSR (2.4 nm in the described device) would be followed by a drift significantly lower than 0.16 nm, which would be tolerable with respect to the bandwidth of the device. This perception is confirmed by previous results obtained on ChG core waveguides [29]: in that experiment we trimmed the resonant wavelength of a ring resonator by 0.35 nm to restore the spectral response of a two-ring filter, and a negligible wavelength drift was observed compared to 0.26 nm bandwidth (32.5 GHz) of the filter. To better clarify the relationship between the induced wavelength shift and the subsequent drift, an extensive investigation is ongoing and results will be reported in future contributions.

Photosensitivity to high-intensity IR light has been previously observed to occur in ChG-based waveguides and circuits above a threshold power density of about $0.1 \text{ GW}/\text{cm}^2$ [36]. We experimentally verified that this threshold is also valid for ChG-assisted silicon waveguides, where no IR sensitivity effects were observed up to a propagating optical power of about 250 mW.

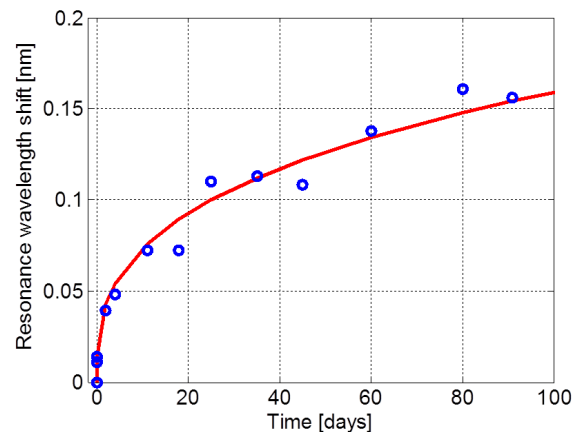


Fig. 5. Time stability of the trimming process of a ChG-assisted SOI ring resonator, when the device is stored in the dark after light exposure: measured (blue circles) resonance wavelength shift and power-law fitting curve (red solid line).

5. Waveguide optimization

The trimming performance reported in the previous section refers to the TE-polarized fundamental mode of standard SOI channel waveguides covered by As_2S_3 cladding. According to numerical simulations of Fig. 1, the maximum effective index change, the corresponding achievable wavelength shift, and the trimming velocity are all expected to double for the TM-polarized fundamental mode of the same waveguides. To further speed up the trimming process and to improve its performance, the waveguide design can be engineered to maximize its sensitivity to light exposure.

To this aim, the effects of photosensitivity on ChG-assisted SOI circuits were numerically investigated as a function of the waveguide dimensions. Figures 6(a) and 6(b) show, respectively, the behaviour of Δn_{eff} and $\Delta\lambda$ versus the core width w , assuming a ChG thickness $t = 420$ nm, as in the fabricated waveguides, and $\Delta n_{As_2S_3} = 4 \cdot 10^{-2}$, as in previous simulations reported in Fig. 1. Since different silicon waveguide cross-sections with thinner core layer were recently proposed and successfully applied [12, 37], we also investigated two different values of core height: $h = 220$ nm (solid lines), as in the realized waveguides, for both TE (blue circles) and TM (red squares) polarizations, and $h = 150$ nm (dashed line), for TE (black circles) polarization.

From Fig. 6 we observe that, for decreasing values of w , the waveguide photosensitivity increases for both polarizations and for both silicon thicknesses. In particular, for $h = 220$ nm, when waveguide width is narrowed from 500 nm (green dashed lines, corresponding to the fabricated waveguides) to 300 nm, the photosensitivity of the TE mode is more than doubled, the Δn_{eff} rising from 0.13 to 0.27 and the $\Delta\lambda$ from 5.7 nm to 12.5 nm. This behaviour is expected: by decreasing w , the fundamental mode becomes less confined and therefore the same amount of ChG cladding refractive index change is able to produce a larger variation of the mode effective index, thus increasing the photosensitivity. However, narrowing the waveguide width also modifies the mode propagation properties and can significantly change the circuit performance. Firstly, the lower confinement factor increases the minimum achievable bending radius and imposes devices with larger footprint and smaller FSR. Secondly, the stronger interaction of the mode with waveguide sidewalls produces, in high-index contrast technology and mainly

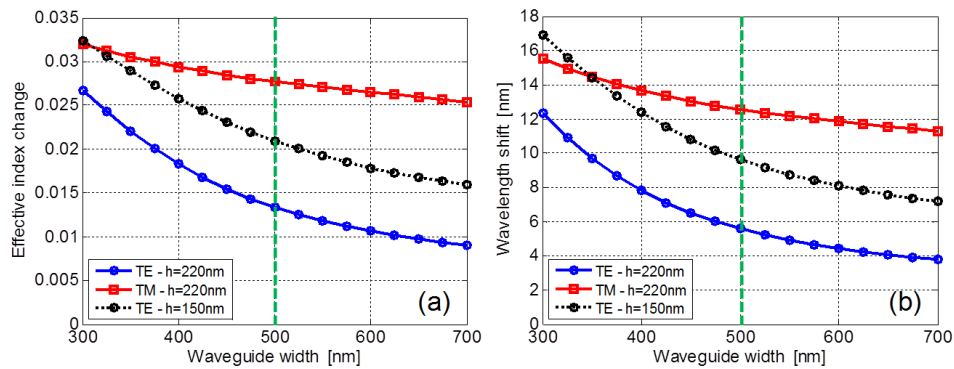


Fig. 6. Numerical simulations of the effects of photosensitivity on ChG-assisted SOI waveguides (ChG thickness $t = 420$ nm, $\Delta n_{As_2S_3} = 4 \cdot 10^{-2}$), versus the width w and height h of the core: (a) effective index variation and (b) corresponding wavelength shift, when $h = 220$ nm (solid lines), for TE (blue circles) and TM (red squares) polarizations, and when $h = 150$ nm (solid lines), for TE (black circles) polarization. Green dashed line corresponds to the value $w = 500$ nm.

in SOI, a remarkable increase of roughness-induced propagation losses and backscattering effects [13]. In contrast, when w is increased above 500 nm, the waveguide loss figure improves, but the photosensitivity decreases and light propagation moves toward multi-mode regime.

Similar considerations hold even when the variation of the silicon core thickness h is analyzed: as h decreases from 220 nm (blue solid line) to 150 nm (black dashed line), the confinement factor worsens and the waveguide photosensitivity improves, but the mode propagation properties change significantly. Assuming, for instance, a waveguide with $w = 500$ nm (green dashed line), both Δn_{eff} and $\Delta\lambda$ of the TE mode increase by a factor 1.6.

This study proves the general validity and flexibility of the proposed approach, enabling to obtain efficiently trimmable circuits from any kind of silicon waveguide structure. The engineering of ChG-assisted waveguides has then to be optimized according to the requirements of each specific application, in order to find the best trade-off between the trimmability of the circuit and its performance in terms of insertion losses, bandwidth, single-mode propagation, and footprint.

6. Conclusion

The discussed experimental results demonstrate ChG-assisted SOI waveguides as a powerful solution to realize easily-, efficiently- and permanently- trimmable PICs.

ChG-assisted SOI circuits can be straightforwardly realized, without additional fabrication steps with respect to the standard process of SOI PICs, simply by using As_2S_3 as upper cladding, rather than SiO_2 .

Compared to alternative approaches, requiring sophisticated and expensive tools [16, 17], the visible light sensitivity of ChG allows the realization of an extremely simple and low-cost trimming technique, employing only a common halogen lamp and an optical fiber. Despite its simplicity, the trimming is highly selective and accurate, enabling local changes in the optical properties of the circuit with a resolution of about 30 μm , that can be easily narrowed by one order of magnitude with a special fiber or a lens. Moreover, it can be easily achieved with real-time monitoring of its effects on the device response.

The achievable trimming range is quite large, comparable or better than the state of the art in the field [16–21], and enough to compensate for typical SOI fabrication tolerances and to completely reconfigure the response of SOI devices over a whole FSR. A photo-induced effective index change of $\Delta n_{eff} = 1.6 \cdot 10^{-2}$ and a wavelength shift of $\Delta\lambda = 6.7$ nm were experimentally demonstrated and these values can be at least doubled by waveguide optimization.

The technique is power-effective, requiring an energy density of only 3 $\text{pJ}/\mu\text{m}^2$ for every nanometer of induced wavelength shift. Even a low-intensity light source is therefore able to produce a fast modification of the circuit: for instance, a wavelength shift of 80 GHz/min can be achieved with a light intensity of only 10 mW/cm^2 . This figure corresponds to a power consumption of only 0.5 μW for each ring resonator that needs to be trimmed. Moreover, since the trimming velocity is proportional to the light intensity, it can be suitably tailored to optimize the trade-off between the time required for the trimming and the desired control on the final circuit performance.

Finally, the induced modifications on the optical properties of the circuits are permanent, enabling a trimming process intrinsically more efficient than common “always-on” tuning mechanisms. Further investigations are ongoing to evaluate under which conditions the small (about 2%) wavelength drift observed after the illumination can be considered negligible or tolerable for the proper behavior of specific devices, that is to evaluate when the presented technique can be used for a “set and forget” trimming of photonic integrated circuits.

ChG-assisted SOI PICs therefore enable a twofold achievement: the compensation for SOI fabrication tolerances to target tight specifications, and the realization of permanently reconfig-

urable PICs avoiding continuous power consumption.

Acknowledgments

The Politecnico di Milano and MIT authors would like to acknowledge the European Office of Aerospace Research and Development (Award No. FA8655-12-1-2051) for partial funding. The Politecnico di Milano and University of Glasgow authors would like to thank the Italian National Project (PRIN) SAPPHIRE.